JOURNAL OF Materials CHEMISTRY

Temperature dependence of the crystal and magnetic structures of the antiferromagnetic oxides $Pb_4Fe_3O_8X$, X = Cl and Br†

Christopher S. Knee and Mark T. Weller*

Department of Chemistry, The University of Southampton, Southampton, UK SO17 1BJ. Tel: 00 44 (0)23 80593592; Fax: 00 44 (0)23 80593592; E-mail: mtw@soton.ac.uk

Received 6th March 2001, Accepted 4th June 2001
First published as an Advance Article on the web 26th July 2001

The crystal and magnetic structures of the antiferromagnetic mineral hematophanite, $Pb_4Fe_3O_8Cl$, and its bromide analogue $Pb_4Fe_3O_8Br$ have been studied over the temperature range 10–650 K using neutron powder diffraction. The materials consist of truncated $Pb_4Fe_3O_8$ triple perovskite blocks separated by a CsCl-type Pb_2X (X = Cl or Br) layer. The basal oxygen of the central FeO_6 octahedra exhibits disorder consistent with alternate clockwise/anticlockwise rotations around the *c*-axis; the degree of rotation increasing upon cooling for both materials, *i.e.* from 10.3° at 650 K to 12.8° at 10 K for $Pb_4Fe_3O_8Br$. The order of the Fe moments evolving as a function of temperature has allowed the $T_{Néel}$ (T_N) of $Pb_4Fe_3O_8Br$ to be determined for the first time as 600(5) K, a value within experimental error of the T_N for $Pb_4Fe_3O_8Cl$. The moments are coupled antiferromagnetically along all three crystallographic directions, resulting in a magnetic structure related to that of the nuclear structure by $a_{mag} = \sqrt{2}a_{nuc}$ and $c_{mag} = 2c_{nuc}$. The magnetic structure is refined with spins perpendicular to the *c*-axis, giving ordered moments of 3.94(3) μ_B for $Pb_4Fe_3O_8Cl$ and 4.10(3) μ_B for $Pb_4Fe_3O_8Br$ at 10 K consistent with the presence of high spin Fe^{3+}.

Introduction

The structure of the rare mineral hematophanite, $Pb_4Fe_3O_8Cl$, was first studied by Rouse[1] who assigned a non-centrosymmetric space group *P*4*mm* to the mineral. Further studies on synthetic $Pb_4Fe_3O_8Cl$ by Pannetier and Batail[2] using single crystal X-ray data concluded the material crystallises with the centrosymmetric space group, *P*4/*mmm*. A subsequent ^{57}Fe Mössbauer investigation by Emery *et al.*[3] revealed the onset of antiferromagnetic order within the Fe spins at a $T_{Néel} \approx 602$ K. The material contains an incomplete triple perovskite $Pb_4Fe_3O_8$ block, with two FeO_5 square pyramids connected through shared apical oxygens to an FeO_6 octahedral site. This arrangement is similar to that found in the well known high T_c material, $YBa_2Cu_3O_{7-\delta}$ (YBCO) and has recently been the focus of several investigations in the Fe substituted, YBCO derivatives, $RBa_2Fe_3O_{8\pm\delta}$ (R = Y, Dy and Er).[4–6] The higher oxidation states favoured by iron in comparison with copper result in full occupancy of all the oxygen sites within these materials. Consequently the Fe ions corresponding to the Cu-chain site are arranged in layers of apex sharing octahedra rather than square planar chains. Neutron powder diffraction[4,6] and Mössbauer studies[5] revealed the Fe moments order antiferromagnetically with $T_{Néel} \sim 650$ K.

In contrast to the lanthanide ion within the $RBa_2Fe_3O_{8\pm\delta}$ triple perovskites, an unusual CsCl-type Pb_2Cl interleaves the magnetically ordered Fe portion of hematophanite. A similar layer has been reported in the lead based cuprate $Pb_3Sr_3Cu_3O_8Cl$ by Cava *et al.*[7] and more recently Rukang synthesised three structural analogues of hematophanite, $Pb_2Sr_2Cu_2TaO_8Cl$,[8] $Pb_2Ba_2Cu_2TaO_8Cl$ and $Pb_2Ba_2Cu_2NbO_8Cl$.[9] These materials contain CuO_5 square pyramids connected through pentavalent MO_6 octahedra, an arrangement commonly observed in the 1212-type superconducting cuprates.[10,11] Further work on these lead halide materials by Crooks *et al.* extended the series with the isolation of Sb^{5+} and Sr/Br derivatives.[12]

In this paper we present the results of a temperature dependent study of hematophanite, and its bromide analogue $Pb_4Fe_3O_8Br$, using neutron powder diffraction. Data has been collected in the range 10–650 K allowing the temperature dependence of the Fe–O coordination to be accurately determined whilst simultaneously monitoring the evolving magnetic structure. The structural data is discussed in relation to the magnetic behaviour of the materials and comparisons with the related $RBa_2Fe_3O_{8\pm\delta}$ phases are made.

Experimental

Synthesis

Stoichiometric amounts of high purity oxides (≥99.95%) PbO, Fe_2O_3 and the lead halides PbX_2 (X = Cl, Br) were intimately mixed and heated in alumina crucibles at 550 °C for 12 h. The samples were then pelletised under ~8 ton cm^{-2} and reacted for 24 h at 650 °C. The phase purity of the powders, $Pb_4Fe_3O_8Cl$ (rusty orange) and $Pb_4Fe_3O_8Br$ (rusty red), was confirmed using a Siemens D5000 diffractometer operating with Cu $K_{\alpha 1}$ radiation.

Powder X-ray diffraction

Further PXD data were collected in the 2θ range 17–117° using a step size of 0.02° and a count time of 12 s. Structural refinement using the Rietveld method[13] and GSAS program,[14] in the space group *P*4/*mmm*, was then performed using the atomic positions reported by Pannetier and Batail[2] as a starting point (Br replacing Cl for $Pb_4Fe_3O_8Br$ analysis). Accurate cell parameters were determined and phase purity confirmed. Introduction of atomic coordinates and thermal parameters revealed deficiencies in the structural model with particularly high temperature factors associated with the Fe(2) and O(3) atoms, *i.e.* the octahedral Fe position and the neighbouring

†Electronic supplementary information (ESI) available: details of refined crystallographic parameters and bond lengths for all temperatures. See http://www.rsc.org/suppdata/jm/b1/b102092g/

 DOI: 10.1039/b102092g

This journal is © The Royal Society of Chemistry 2001

in-plane oxygen. The results are indicative of site disorder and it is noteworthy that an anomalously high thermal parameter for the O(3) atom was also observed by Pannetier and Batail in their single crystal X-ray study of $Pb_4Fe_3O_8Cl$.[2] The limitations of X-ray diffraction in accurately locating oxygen positions led us to collect and analyse powder neutron diffraction (PND) data on the materials.

Neutron powder diffraction

The samples ($\sim$15 g) were placed in 17 mm diameter vanadium cans and room temperature data collected on the high resolution diffractometer, D2B, at the Institut Laue Langevin (ILL), Grenoble, operating with the optimum wavelength $\lambda = 1.594$ Å. Low temperature scans (10 and 150 K) were performed in a standard ILL cryostat and high temperature runs (400, 450, 500, 520, 540, 560, 580, 600 and 650 K) using a niobium furnace. A temperature stability of ± 2 K was maintained throughout the range. The size of the samples and the large scattering cross sections of Pb and Fe meant a collection time of 1 h at each temperature was adequate.

Results

Crystal structure refinement

The powder patterns were analysed using the GSAS program[14] with the nuclear scattering lengths taken to be Pb = 9.40, Fe = 9.54, Br = 6.79, Cl = 9.58 and O = 5.81 fm.[15] Initial cycles introduced background parameters, histogram scale factor, profile coefficients and lattice constants to give a reasonable fit to the data. However, additional intensity arising from the antiferromagnetic order of the Fe spins (particularly strong at high *d*-spacings and low temperatures) was apparent for both materials in scans run below 600 K. The reflections were found to be consistent with a magnetic cell related to that of the nuclear structure by $a_{mag} = \sqrt{2}a_{nuc}$ and $c_{mag} = 2c_{nuc}$ and were fitted by introducing the magnetic model as a second phase. Further details of the refinement of the magnetic structure are given in the following section. Analyses of the crystal structures proceeded with the variation of positional and thermal parameters for the individual atoms. The temperature factors all refined to acceptable values with the exception of the O(3) oxygen, that lies in the basal plane of the $Fe(2)O_6$ octahedra. The thermal parameter (B_{iso}) refined to an unacceptably high value of $\sim$8 Å^2 at 10 K for both $Pb_4Fe_3O_8Cl$ and $Pb_4Fe_3O_8Br$. Such a value is incompatible with the low temperature of data collection and indicates positional disorder or possible partial occupancy of the site. The latter scenario was checked by allowing the fractional occupancy of the O(3) atom to vary, however this had a negligible effect on the least squares statistics and the site remained at full occupancy within experimental uncertainty. In contrast the introduction of an anisotropic temperature factor for the oxygen produced a significant improvement in the fit, revealing a large ($\beta_{11} =$ 24.5 Å^2 for $Pb_4Fe_3O_8Cl$) component along the *x*-direction. The scattering from this site was therefore modelled by displacing the atom along *x* on to a half occupied *4o* site, (*x*,½,½) with $x \approx 0.1$. This arrangement refined smoothly to produce realistic positional and thermal parameters and was repeated for all the data sets. Similar displacements are commonly observed in multilayer perovskites[10–12] and in this case represent a rotation of the rigid FeO_6 octahedra about the *c*-axis. In the absence of appreciable oxygen deficiency weak $\sqrt{2}a \times \sqrt{2}a$ superlattice peaks arising from extended regions of correlated clockwise/anticlockwise rotations are sometimes observed using neutron diffraction.[10,11] However, the $Pb_4Fe_3O_8X$ materials are unusual since at temperatures below 600 K the ordered Fe moments lead to a $\sqrt{2}a \times \sqrt{2}a \times 2c$ magnetic cell giving magnetic peaks coincident with possible oxygen superlattice reflections. Further comments on the presence or otherwise of a supercell within the compounds, and the structural implications of the split O(3) site are made in the discussion.

Table 1 Refined structural parameters for $Pb_4Fe_3O_8X$, X = Cl and Br, at 295 K. Space group *P4/mmm*, no. of observations = 2868, no. of variables = 42, and $Z = 1$

Atom	Site	(*x*,*y*,*z*)		$Pb_4Fe_3O_8Cl$	$Pb_4Fe_3O_8Br$
Pb(1)	*2h*	(½,½, *z*)	*B*/Å^2	0.61(3)	0.59(3)
			z	0.1197(1)	0.1268(1)
Pb(2)	*2h*	(½,½,*z*)	*B*/Å^2	0.86(3)	0.85(3)
			z	0.3800(1)	0.3823(1)
Fe(1)	*2g*	(0,0,*z*)	*B*/Å^2	0.44(3)	0.40(3)
			z	0.2443(1)	0.2490(1)
Fe(2)	*1b*	(0,0,½)	*B*/Å^2	0.43(4)	0.41(3)
O(1)	*4i*	(0,½,*z*)	*B*/Å^2	0.69(3)	0.71(3)
			z	0.2110(1)	0.2165(1)
O(2)	*2g*	(0,0,z)	*B*/Å^2	1.05(5)	0.96(4)
			z	0.3669(2)	0.3688(2)
O(3)	*4o*	(x,½,½)	*B*/Å^2	0.70(6)	0.59(6)
			x	0.1069(8)	0.1052(8)
			n	0.5	0.5
X	*1a*	(0,0,0)	*B*/Å^2	1.51(6)	1.09(6)
a/Å				3.91476(7)	3.92347(4)
c/Å				15.3088(3)	15.5687(2)
μ/μ_B[a]				3.55(3)	3.52(3)
R_p (%)				4.76	5.04
R_{wp} (%)				6.40	6.81
χ^2				1.35	1.56

[a]Magnetic unit cell: space group *Imm'm*; $a_{mag} = b_{mag} = \sqrt{2}a_{nuc}$ and $c_{mag} = 2c_{nuc}$; $|\mu| = \mu_x$, $\mu_y = \mu_z = 0$. Refinement constrained to μ_x Fe(1) = μ_x Fe(2).

The final stages of the refinements probed the occupancy of the oxygen sites but they did not show a statistically significant ($> 3\sigma$) decrease. The refined structural parameters of the two materials at room temperature are listed in Table 1, and selected interatomic distance and bond angles shown in Table 2. The final fit for $Pb_4Fe_3O_8Cl$ at 10 K is shown in Fig. 1.

Magnetic structure refinement

The onset of antiferromagnetic order in $Pb_4Fe_3O_8Cl$ at a $T_N \approx 602$ K,[3] indicated that the additional reflections in data sets recorded below 600 K were due to the ordered Fe moments. The peaks were found to be consistent with a magnetic cell related to that of the nuclear structure by the transformation matrix (10/110/002). This behaviour is identical to that observed by Karen *et al.*[6] in their investigation of the related $RBa_2Fe_3O_{8+\delta}$ triple perovskite series in which nearest

Table 2 Selected derived bond distances (Å) and angles (°) for $Pb_4Fe_3O_8X$, X = Cl and Br at 295 K. For Pb(1)–X–Pb(1) bonds (see also Fig. 6)

Bond	$Pb_4Fe_3O_8Cl$	$Pb_4Fe_3O_8Br$	
Pb(1)–O(1)	2.4048(15)	2.4083(15)	×4
Pb(1)–X	3.3198(10)	3.4050(11)	×4
Pb(2)–O(1)	3.244(2)	3.242(2)	×4
Pb(2)–O(2)	2.7753(3)	2.7823(3)	×4
Pb(2)–O(3)	2.397(2)/3.003(3)	2.399(2)/2.999(3)	×4
Fe(1)–O(1)	2.0226(7)	2.0256(7)	×4
Fe(1)–O(2)	1.879(4)	1.866(4)	×1
Fe(2)–O(2)	2.037(3)	2.043(3)	×2
Fe(2)–O(3)	2.0016(7)	2.0047(7)	×4
O(1)–Fe(1)–O(1)	150.83(15)	151.14(14)	
O(3)–Fe(2)–O(3)	155.9(2)	156.2(2)	
Pb(1)–X–Pb(1) [i]	67.01(5)	70.87(5)	
Pb(1)–X–Pb(1) [ii]	72.26(3)	70.36(3)	

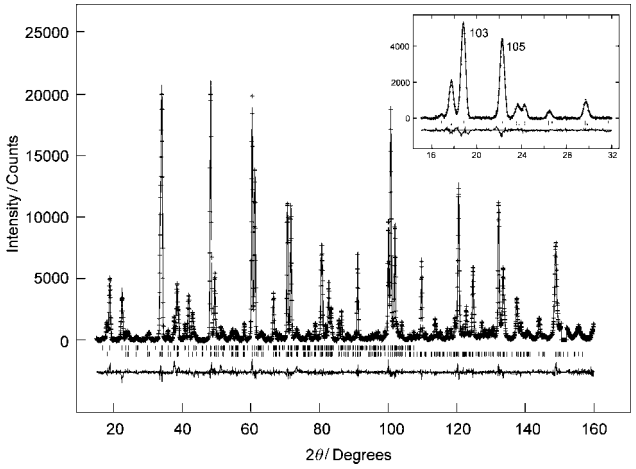

Fig. 1 Final fit to the neutron powder diffraction data of $Pb_4Fe_3O_8Cl$ collected at 10 K. Data points are marked as crosses, profile fit as the upper continuous line and difference as the lower continuous line. The lower (upper) set of reflection markers refer to the nuclear (magnetic) structure. Inset shows fit achieved to most intense 103 and 105 magnetic reflections.

neighbour Fe moments are coupled antiferromagnetically along all three crystallographic directions with spins lying perpendicular to the *c*-axis. Adopting this model results in the magnetic symmetry of the $Pb_4Fe_3O_8X$ materials becoming orthorhombic, space group *Imm'm*.

The magnetic model was introduced into the refinements as a secondary phase using a calculated magnetic form factor for Fe^{3+}.[16] The orientation of the iron spins within the *xy*-plane cannot be determined in our powder diffraction experiment and was therefore fixed arbitrarily along the *a*-axis. Initially the Fe moments of the two sites were constrained to be equal. This arrangement refined to give ordered components of $\mu_x = 3.94(3)\ \mu_B$ and $\mu_x = 4.10(3)\ \mu_B$ at 10 K for $Pb_4Fe_3O_8Cl$ and $Pb_4Fe_3O_8Br$ respectively, and good agreement between observed and calculated magnetic intensities (see inset to Fig. 1). Attempts to vary the individual moments of the two sites produced the following results; for the $Pb_4Fe_3O_8Br$ analyses the Fe(1) and Fe(2) moments remained within experimental uncertainty but for the $Pb_4Fe_3O_8Cl$ refinements, they diverged to give an unrealistically high value of 5.92(4) μ_B on the octahedral Fe(2) position and 2.61(3) μ_B for Fe(1) at 10 K. The disparity most likely reflects the high degree of correlation between the two parameters and therefore the values presented were those obtained from the constrained refinement. The presence of a *z* magnetic component can not be ruled out from our analysis, however refinements performed with the moment aligned solely along *z* produced a deterioration in the fit indicating that the adopted model is an accurate representation of the magnetic order within the materials.

The expected decrease in the magnitude of the antiferromagnetic moment (μ_{AF}) occurred with increasing temperature. Fig. 2 shows the temperature dependence of the normalised intensity of the strongest magnetic reflection, the 103, for the materials whilst Fig. 3 plots the refined μ_{AF} values as a function of temperature. It should be noted that above 560 K the magnetic intensity diminished rapidly, leading to increased uncertainty in the derived moments.

Discussion

The large amount of data collected on the two materials necessitates the division of the discussion into four sections: First the main points of the crystal structure determination are discussed, second the structural differences arising from replacing the Pb_2Cl layer with Pb_2Br are highlighted. Third

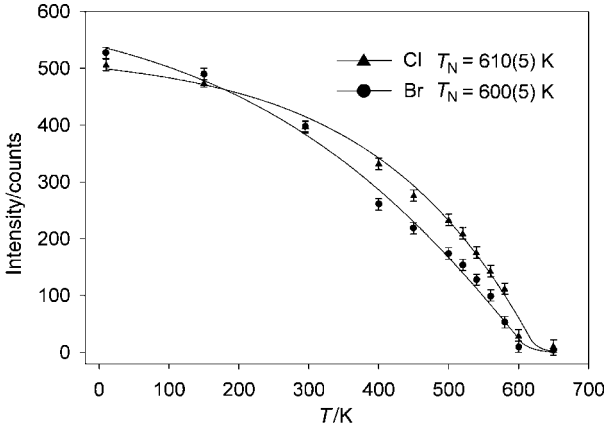

Fig. 2 Temperature variation of the intensity of the magnetic reflection 103 (nuclear 1/2, 1/2, 3/2) for $Pb_4Fe_3O_8X$ (X = Cl and Br).

the temperature dependences of both structures are analysed and finally results of the magnetic refinement are presented.

Crystal structure

The truncated triple perovskite block within hematophanite and its bromide analogue $Pb_4Fe_3O_8Br$ exhibit a high degree of structural distortion (see Fig. 4). In particular a significant horizontal displacement of the basal O(3) oxygen ~0.5 Å of the central $Fe(2)O_6$ octahedra is observed. Table 2 shows the distortion reduces the in-plane O(3)–Fe(2)–O(3) bond angle from the ideal 180° to a value close to 156° for both materials at room temperature. Physically the displacement represents a rotation of the Fe-octahedra about the *c*-axis, *e.g.* by *ca.* 12° for both compounds. The disorder is believed to be a consequence of the structure alleviating bond strain. It has the effect of lengthening the in-plane Fe(2)–O(3) distances for a fixed *a* lattice parameter; *e.g.* for $Pb_4Fe_3O_8Cl$ at room temperature an ideal O(3) site of (0,½,½) would produce an Fe(2)–O(3) distance of 1.957 Å (*i.e.* *a*/2) but with the displacement this increases to 2.004 Å. Bond valence calculations[17] show the elongation of the Fe–O basal interaction is more compatible with Fe^{3+} occupying the octahedral site. Without the disordered position calculations predict an Fe valence of 3.30 for $Pb_4Fe_3O_8Cl$ and 3.28 for $Pb_4Fe_3O_8Br$, with the split site this drops to 3.03 and 3.02 for the chloride and bromide materials respectively.

Displacement of the basal oxygen in the MO_6 octahedra of the same magnitude has been observed in the cuprate hematophanite analogues, $Pb_2(Ba/Sr)_2Cu_2M'O_8X$, M' = Nb, Ta, Sb; X = Cl, Br[9,12] and similar structural disorder is commonly reported in multiple B cation cuprate perovskites.[10,18] In

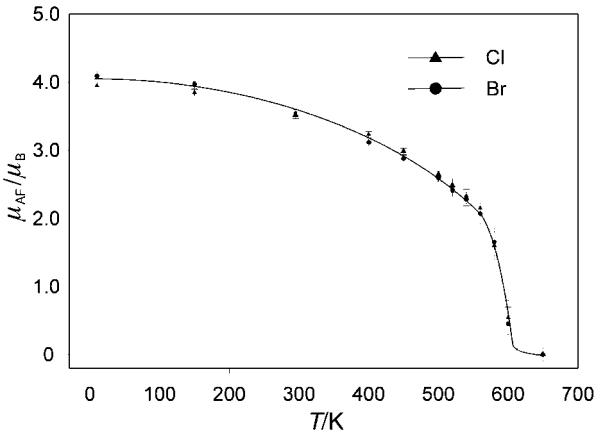

Fig. 3 Temperature dependence of the ordered Fe moment (μ_{AF}) in the $Pb_4Fe_3O_8X$ (X = Cl and Br) materials.

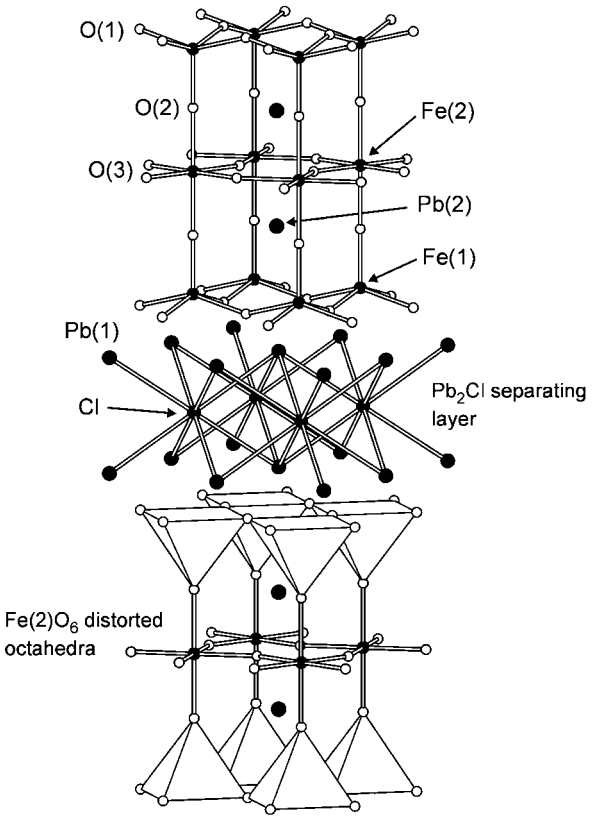

Fig. 4 The structure of $Pb_4Fe_3O_8Cl$. The square pyramidal Fe(1) and octahedral Fe(2) positions are shown bonding to their respective oxygen atoms in the top half of the diagram and the chloride ion is shown bonding 8-fold to the lead atoms forming a Pb_2Cl layer.

these materials the disorder may arise due to the incompatibility of the sizes of the cuprate and other B cation layers or be caused by the highly charged, strongly polarising B′ cation. These explanations do not account for the oxygen disorder observed in the triple Fe–O perovskite block in the materials currently under investigation. A more likely origin of the disorder is the requirement of nominal Fe^{3+} to adopt two distinct geometries. The displacement may provide a way of reconciling the shorter planar Fe–O interaction of the $Fe(1)O_5$ square pyramids with the basal plane of the $Fe(2)O_6$ octahedra. Alternatively, the distortion may be a result of the Pb(2) ion preferring to adopt a non-regular environment. Whatever the exact reason for the O(3) displacement it is interesting that comparable disorder has not been observed within the basal FeO_2 plane of the equivalent FeO_6 octahedra in the $RBa_2Fe_3O_{8\pm\delta}$ phases.[6]

Introducing the split site within *P*4/*mmm* symmetry corresponds to a fully disordered situation, *i.e.* a 50 : 50 arrangement of clockwise and anticlockwise rotations. It is unlikely that such disorder occurs over a very short-range within the materials, as it would require significant distortions of the corner sharing octahedra. Instead extended regions are likely to exist where neighbouring octahedra rotate in opposing directions as shown in Fig. 5. If the domains are large enough then such behaviour may lead to the observation of superlattice reflections. The presence of magnetic intensity complicates the situation for the $Pb_4Fe_3O_8X$ materials and places added importance on the data collected at 650 K, $\sim$50 K above the antiferromagnetic transition. Careful inspection of this data for both materials has revealed no evidence of supercell reflections, indicating that the size of the alternating clockwise/anticlockwise domains must be limited to at most a few hundred Ångstroms before the phase of the rotations is reversed. Previous neutron diffraction studies on the related $Pb_2(Ba/Sr)_2Cu_2M'O_8X$ phases (M′ = Nb, Ta and Sb) revealed

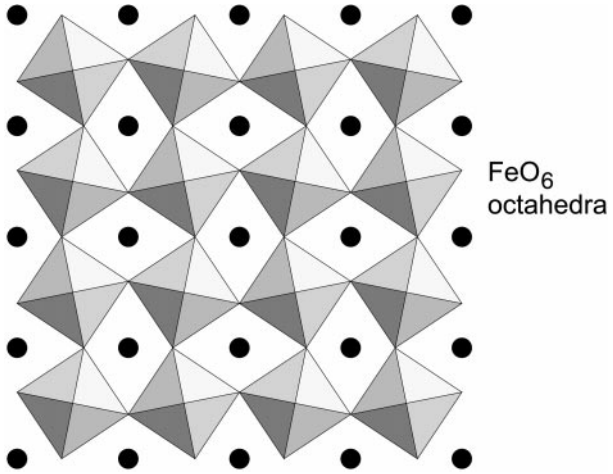

Fig. 5 Schematic model for the rotations of the FeO_6 octahedra around *c* in the $Pb_4Fe_3O_8Cl$ structure. The diagram shows a domain of oppositely aligned octahedra.

rotations of the MO_6 octahedra, by $\sim12^\circ$ for Ba and $\sim14^\circ$ for Sr derivatives, but also failed to detect supercell intensity.[12]

This behaviour is somewhat different to that reported for the YBCO related superconductor, $RuSr_2GdCu_2O_8$.[11] This compound contains regions of zigzagging RuO_6 octahedra which give rise to weak $\sqrt{2}a\times\sqrt{2}a\times c$ superstructure peaks in both neutron and electron diffraction data.[11,19] This observation probably reflects differences in the microstructure of the two types of materials. At elevated temperature increased thermal motion will result in a fully disordered configuration for both materials, however quenching the $Pb_4Fe_3O_8X$ samples rapidly in air effectively freezes in the disorder. Conversely the prolonged oxygen annealing and slow cooling employed in the synthesis of the ruthenium–cuprate is likely to promote oxygen ordering, giving rise to domains of a particular sense of rotation large enough to be observed by neutron diffraction. In addition the weaker interactions involving the Pb(1)–halide layer will lead to more stacking faults along the *c*-direction within the $Pb_4Fe_3O_8X$ compounds, further reducing three dimensional structural correlations necessary for observation in diffraction experiments.

In contrast to the horizontal distortion within the Fe(2)–O(3) plane, the square pyramidal Fe(1) position lies approximately 0.5 Å above/below the O(1) basal plane, giving a O(1)–Fe(1)–O(1) bond angle $\sim151^\circ$ for both materials. Bond valence calculations performed on this site reveal a marked difference between the valence of the octahedral Fe(2) (3.03 and 3.02 valence units for Cl and Br, respectively) and pyramidal Fe(1) (2.60 and 2.71 respectively). Such a low valence for Fe(1) might imply that further anions are required in its coordination sphere, however, this is unlikely given the proximity of the halide ion. A more probable explanation for the calculated Fe(1) valence being lower than expected is that the bond valence parameters are not entirely reliable since the bonding is under significant strain.

The second interesting feature of the crystal structure is the interleaving, Pb_2X (X = Cl, Br), layer. Adopting the nomenclature used to describe the high T_c cuprates this layer is referred to as a separating layer since it separates the basal planes of the two $Fe(1)O_5$ square based pyramids (CuO_5 pyramids in high T_c oxides). The Pb_2X layer is derived from the CsCl structure with Pb replacing Cs at the corners of an approximate cube in the materials. Fig. 6 provides a closer view of the Pb–chloride coordination present in hematophanite, showing the Pb(1)–Cl bond and the two Pb(1)–Cl–Pb(1) bond angles. The thickness of the Pb_2Cl block, as estimated from the Pb(1) to Pb(1) separation is also shown.

The geometry of the Pb(2) site, which bonds to all three

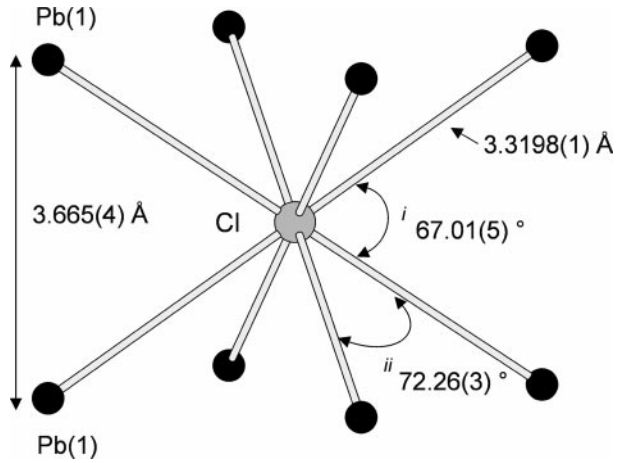

Fig. 6 The Pb_2Cl separating layer present in $Pb_4Fe_3O_8Cl$. Pb(1)–Cl and Pb(1)–Pb(1) distances are indicated along with selected bond angles (see also Table 2).

oxygen positions, is formally 12-fold cubo-octahedral. The coordination is, however, far from regular with the ions lying much closer to the octahedral Fe(2) basal plane. This displacement was noted by Pannetier and Batail[2] and attributed to electrostatic repulsion between Pb(1) and Pb(2). The atom also bonds to the disordered O(3) atom which further complicates the coordination. Similar non-uniform Pb–O environments are often observed, for example in the highly distorted perovskite $PbZrO_3$.[20]

A comparison of the interatomic distances determined for $Pb_4Fe_3O_8Cl$ at room temperature in this study with those of reference 2 shows a number of significant differences particularly in the Fe–O coordination. The effect of refining a split O(3) site is clearly reflected in the increased Fe(2)–O(3) distance, *i.e.* 2.0016(7) Å compared with the previously reported 1.9548(1) Å. In addition the two apical interactions show important differences, with the Fe(1)–O(2) bond being considerably shorter in our analysis, *i.e.* 1.878(4) Å *cf.* 1.932(39) Å and the Fe(2)–O(2) distance an identical amount larger, *i.e.* 2.037(3) Å *cf.* 1.983(35) Å. To check whether these differences were solely a consequence of the disordered O(3) site the results of a refinement with an anisotropic thermal parameter in place of the split position were analysed. However this gave a marginally shorter Fe(1)–O(2) bond and longer Fe(2)–O(2) bond, accentuating the discrepancy. The most probable explanation is that the increased sensitivity of neutron diffraction with respect to oxygen, as shown by the reduced esd's, has allowed us to determine the Fe–O coordination more accurately than the previous single crystal study.

The occupancy of the oxygen sites was also investigated during the refinement process and confirmed the compounds to be oxygen stoichiometric. Simple valence counting, assuming no Pb^{4+}, therefore requires a nominal Fe oxidation state of +3 in $Pb_4Fe_3O_8Cl(Br)$ to maintain charge neutrality but gives no information about the relative magnitude of the valence of the two sites. The exact Fe valence of the equivalent positions within the $RBa_2Fe_3O_{8\pm\delta}$ ($\delta \approx 0$) series remains an area of uncertainty; with Mössbauer studies suggesting the sites are both trivalent, R = Dy, Er and Y,[5] or differ appreciably, R = Y[21] depending on the material/interpretation. Further comments regarding the Fe valence and associated moment of the title compounds are made below in the discussion of their magnetic structures.

Effect of chloride to bromide substitution

Replacing the chloride ion (ionic radius = 1.81 Å, 6-fold coordination[22]) in the Pb_2X layer in hematophanite by the larger bromide ion (ionic radius = 1.96 Å[22]) produces the expected expansion in cell volume, with the a parameter increasing by ~0.01 Å and a greater 0.25 Å enlargement along c (Table 1). The expansion in a is reflected in the basal Fe(1)–O(1) and Fe(2)–O(3) bonds which show an increase in length ~0.004 Å, consistent with the overall trend. Interestingly the level of rotation of the $Fe(2)O_6$ octahedra at room temperature is not greatly affected, *i.e.* 12.1(2)° for hematophanite and 11.9(2)° for $Pb_4Fe_3O_8Br$.

The apical interaction of the FeO_6 octahedra, Fe(2)–O(2), shows a small increase, however the apical Fe(1)–O(2) distance reveals a surprising contraction, *e.g.* from 1.879(4) Å in $Pb_4Fe_3O_8Cl$ to 1.866(4) Å in $Pb_4Fe_3O_8Br$ from the 295 K data. As a result the $Fe(1)O_5$–$Fe(2)O_6$–$Fe(1)O_5$ triple perovskite block within $Pb_4Fe_3O_8Br$ shortens by ~0.015 Å across the whole temperature range. This runs contrary to the observed 0.25 Å increase in the c cell constant and suggests the perovskite block is under compressive strain along the z-direction in $Pb_4Fe_3O_8Br$. The source of the strain, and the larger c-parameter, is the significant elongation of the Pb_2X layer that occurs when Cl^- is replaced by Br^-. The expansion is a result of the large increase in the Pb(1)–X bond from 3.319 Å in $Pb_4Fe_3O_8Cl$ to 3.408 Å in $Pb_4Fe_3O_8Br$. Consequently the thickness of the Pb_2X layer increases from 3.67 Å in $Pb_4Fe_3O_8Cl$ (Fig. 6) to 3.94 Å in $Pb_4Fe_3O_8Br$. The expansion is also reflected in the geometry of the layer, giving a vertically elongated cube when the central position is occupied by the bromide ion in comparison with a flattened cube in $Pb_4Fe_3O_8Cl$. The same trend of a vertically squashed cube for the Pb_2Cl layer and an elongated cube for the Pb_2Br block is seen in the $Pb_2(Ba/Sr)_2Cu_2M'O_8X$, X = Cl, Br materials.[12]

Temperature dependence of the structures

The cell constants of the two compounds show a smooth, monotonic variation with temperature, Figs. 7 and 8. Both phases show a remarkably consistent 0.03 Å increase in the a parameter and a 0.17 Å expansion along c over the 10–650 K temperature range. Comparing the percentage change in the a and c parameters for the materials shows similar increases of ~0.8% for a and 1.1% for c. This is in good agreement with the results of reference 2, and indicates that the thermal expansion is not very anisotropic, surprising for layered materials which usually exhibit significantly greater expansion in the direction perpendicular to the planes.

The temperature dependence of the derived interatomic distances, particularly the Fe–O bond lengths reveals a more complex behaviour, Figs. 9–13. The planar Fe(1)–O(1) interactions for both materials (Fig. 9) show the expected contraction on cooling, *i.e.* ~0.015 Å, mirroring that observed for the a-parameters. In contrast the basal planes of the $Fe(2)O_6$ octahedra exhibit a differing behaviour depending on the

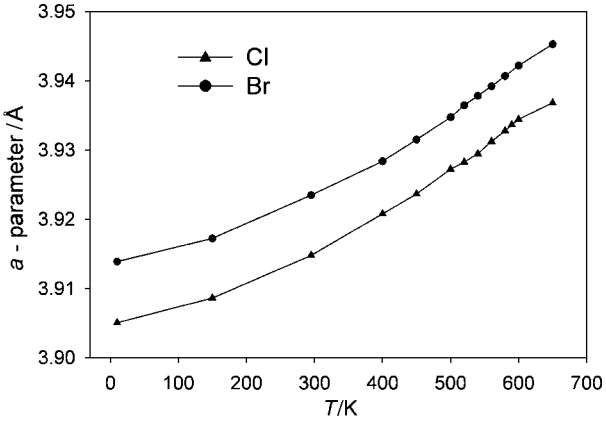

Fig. 7 Temperature dependence of the a-parameter of $Pb_4Fe_3O_8Cl$ and $Pb_4Fe_3O_8Br$.

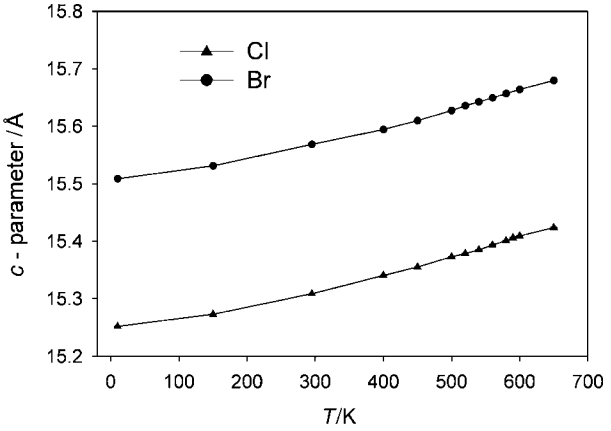

Fig. 8 Temperature dependence of the *c*-parameter of $Pb_4Fe_3O_8Cl$ and $Pb_4Fe_3O_8Br$.

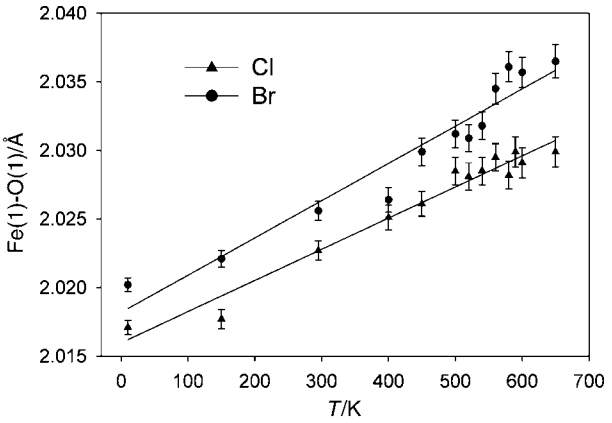

Fig. 9 The Fe(1)–O(1) distances as a function of temperature.

halide; the hematophanite Fe(2)–O(3) bond decreasing slightly from 10 to 400 K before increasing to a plateau of ~2.004 Å and that of $Pb_4Fe_3O_8Br$ which shows no overall expansion, Fig. 10. The magnitude of the O(3) displacement is of course critical in determining the Fe(2)–O(3) distance and the degree of rotation the octahedron experiences. It is therefore beneficial to consider simultaneously Fig. 10 and Fig. 11, which shows the level of rotation decreasing with temperature for both materials, indicative of an increase in bond strain at lower temperatures which is alleviated by greater rotation of the $Fe(2)O_6$ octahedra. This increased rotation at lower temperatures allows the Fe(2)–O(3) bond in $Pb_4Fe_3O_8Br$ to remain constant across the 640 K range and exhibit such a small overall increase ~0.003 Å for $Pb_4Fe_3O_8Cl$. The materials exhibit a near identical degree of rotation at 10 K, *i.e.* 12.8(2)°,

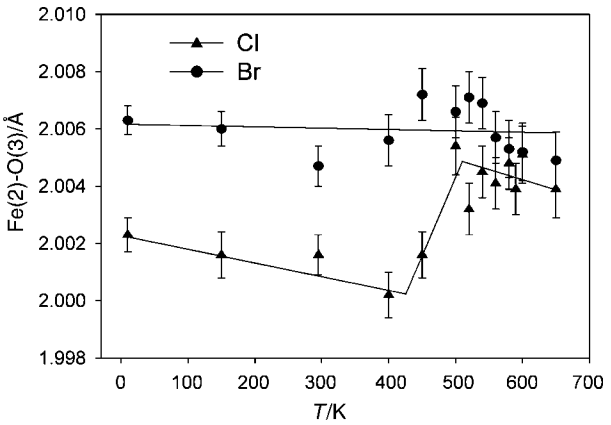

Fig. 10 The Fe(2)–O(3) distances as a function of temperature.

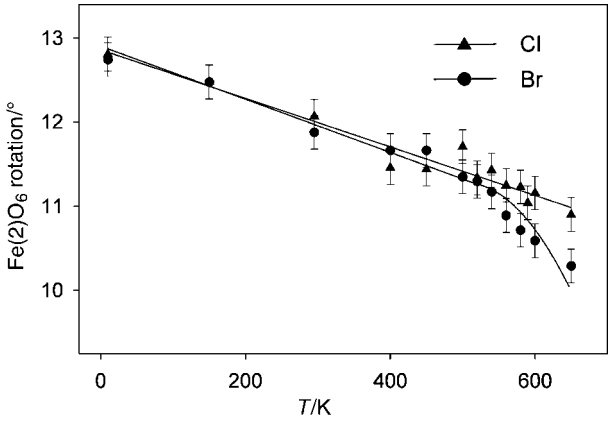

Fig. 11 Rotation angles of the $Fe(2)O_6$ octahedra about the *c* axis *vs.* temperature.

but it appears the level of bond strain present in $Pb_4Fe_3O_8Br$, and hence the degree of rotation needed to alleviate it, decreases at temperatures above 500 K, *e.g.* a value of 10.3° at 650 K compared with 10.9° for $Pb_4Fe_3O_8Cl$. Fig. 11 clearly shows the divergence in the amount of rotation the FeO_6 octahedron experiences; with the rotation remaining at a constant rate in $Pb_4Fe_3O_8Cl$ but decreasing in the Br analogue.

It is difficult to explain the sharp increase in the Fe(2)–O(3) distance for $Pb_4Fe_3O_8Cl$ that occurs between 400 and 500 K, it may reflect that over this temperature range the expansion of the Fe(2)–O(3) bond is too great to be counteracted by rotation of the octahedra. Alternatively it may be a weak magnetostriction as magnetic order grows within the phase.

Plots of the Fe–O(2) apical bonds (Figs. 12a and 12b) show the expected expansion for the Fe(2)–O(2) increasing by ~0.04 Å, however the Fe(1)–O(2) interaction remains constant for both compounds. In fact the coordination of the $Fe(1)O_5$ square pyramid is remarkably static over the temperature range, with the buckling O(1)–Fe(1)–O(1) angle also remaining

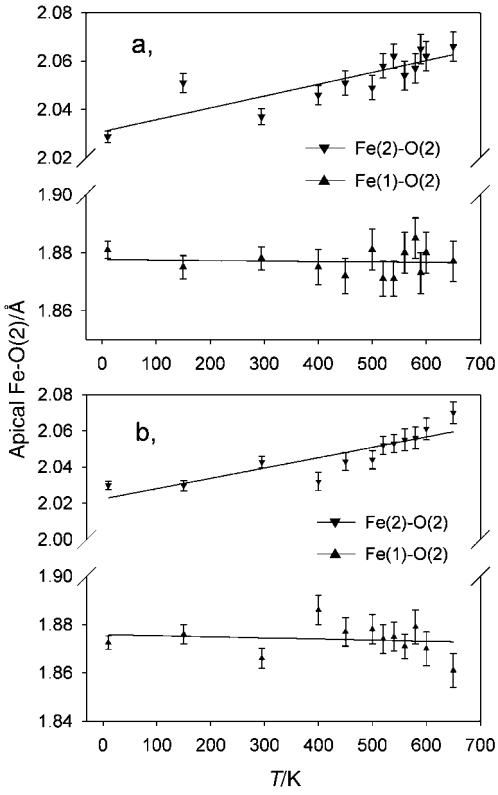

Fig. 12 Temperature dependence of the apical Fe(1)–O(2) and Fe(2)–O(2) bonds of $Pb_4Fe_3O_8Cl$ (a) and $Pb_4Fe_3O_8Br$ (b).

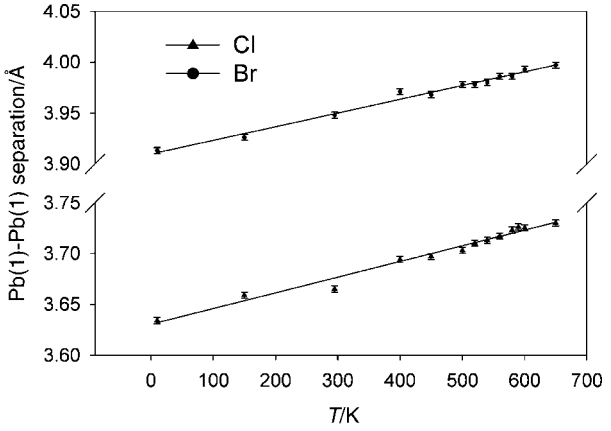

Fig. 13 Temperature dependence of the Pb(1)–Pb(1) separation in the $Pb_4Fe_3O_8X$ materials.

static at a value of ~151°. Only the Fe(1)–O(1) distance changes to any great degree. The increase in the Fe(2)–O(2) bonds accounts for approximately half the observed expansion along *c*, the rest is a result of the thermal expansion in the Pb(1)–halide bond which leads to the thickness of the Pb_2X layer increasing; from 3.63 Å at 10 K to 3.73 Å at 650 K in $Pb_4Fe_3O_8Cl$ and a similar extension for $Pb_4Fe_3O_8Br$, Fig. 13.

Magnetic structure

The high magnetic order onset temperature of $Pb_4Fe_3O_8Cl$, $T_{Néel}=602$ K,[3] indicates the existence of a strong interaction within and between the Fe–O layers of the material. The intense magnetic reflections observed in the neutron powder diffraction patterns of hematophanite and $Pb_4Fe_3O_8Br$ collected below 500 K also indicate the presence of a large, long-range ordered, moment, behaviour which mirrors that previously determined for the $RBa_2Fe_3O_{8+\delta}$ phases,[4,6] and produces a magnetic cell related to that of the nuclear structure by $a_{mag}=\sqrt{2}a_{nuc}$ and $c_{mag}=2c_{nuc}$. Given the presence of the same FeO_5–FeO_6–FeO_5 repeat unit within both sets of materials, this observation is perhaps not surprising.

The magnetic order parameters for both $Pb_4Fe_3O_8X$ compounds are shown in Fig. 2. The data allows the T_N of $Pb_4Fe_3O_8Cl$ to be determined as 610(5) K in good agreement with the previously reported value.[3] The T_N of $Pb_4Fe_3O_8Br$ is estimated to be a little lower at 600(5) K. As discussed above the effect on the structure, particularly the Fe–O sublattice, caused by replacing the chloride ion by bromide is quite small and a similar ordering temperature is therefore expected. The $T_{Néel}$s observed for the $RBa_2Fe_3O_{8+\delta}$ triple perovskites also remain constant at ~650 K despite variation in the lanthanide size.[6]

The ordered moments (μ_{AF}) for $Pb_4Fe_3O_8Cl$ and $Pb_4Fe_3O_8Br$ remain very similar over the experimental temperature range (see Fig. 3), with the latter compound having a marginally greater moment at 10 K of 4.10(3) μ_B compared with 3.94(3) μ_B for hematophanite. These values were derived from a constrained model, *i.e.* μ_{AF} Fe(1) = μ_{AF} Fe(2), and with the orientation of the iron spins fixed arbitrarily along the *a*-axis, giving the arrangement shown in Fig. 14. The previous Mössbauer study of $Pb_4Fe_3O_8Cl$[3] indicated that there are slightly different critical exponents β for the two magnetic layers. However this difference is too small to be detected in our neutron diffraction experiments. The large magnitude of the ordered moments indicates the presence of high spin Fe^{3+} within $Pb_4Fe_3O_8Cl$ and $Pb_4Fe_3O_8Br$. This, coupled with the absence of any oxygen deficiency, leads us to believe that the Fe valence on both sites is +3.

The refined moments at room temperature ($\mu=3.55(3)$ μ_B, Cl and $\mu=3.52(3)$ μ_B, Br) are slightly higher than those

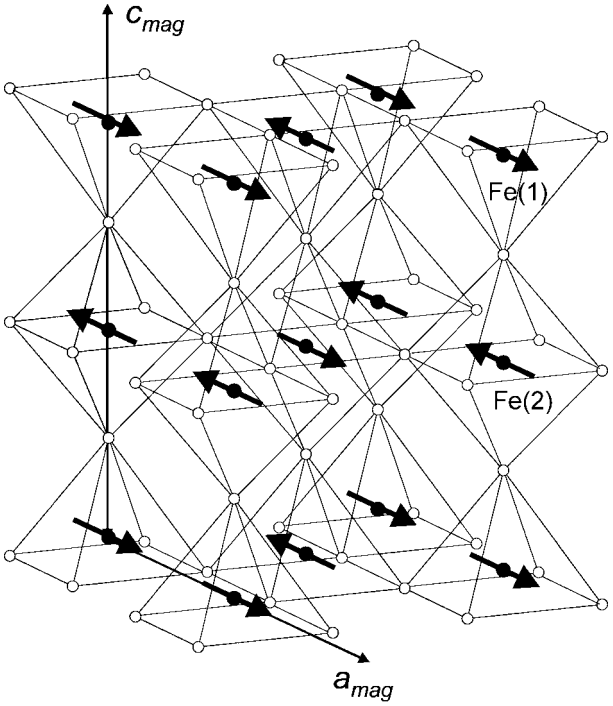

Fig. 14 A section of the magnetic unit cell of $Pb_4Fe_3O_8Cl$ showing the antiferromagnetically ordered iron spins aligned along the *a*-direction.

determined for the $RBa_2Fe_3O_{8+\delta}$ series: R = Y, $\mu=3.43(3)$ μ_B, R = Dy, $\mu=3.27(3)$ μ_B and R = Er, $\mu=3.41(2)$ μ_B at 296 K.[6] Conversely the $T_{Néel}$s in the $Pb_4Fe_3O_8X$ materials are some 50 K lower than those exhibited by the $RBa_2Fe_3O_{8+\delta}$ phases. The differences are quite small, suggesting that the spontaneous onset of magnetism within these layered Fe-oxides is relatively insensitive to the size and type of the separating layer present, *i.e.* the Fe(1) to Fe(1) distance across the lead–halide layer in the $Pb_4Fe_3O_8X$ materials at 7.44 Å (X = Cl) and 7.57 Å (X = Br) is almost double the 3.81 Å in $YBa_2Fe_3O_8$.

Another significant structural difference between the two systems which has implications for the strength of the magnetic interaction and the electrical properties of the title compounds is the disorder within the basal plane of the Fe(2)O_6 octahedra. This leads to a reduction in the critical Fe(2)–O(3)–Fe(2) exchange angle from 180° to 156°, *i.e.* intermediate between a non-distorted perovskite and the type of M–O–M interaction found in pyrochlores. The distortion reduces orbital overlap and tends to favour a localisation of electrons compatible with the high resistivity displayed by $Pb_4Fe_3O_8Cl$.[2]

Conclusions

The evolution of the crystal and magnetic structures of the mineral, $Pb_4Fe_3O_8Cl$, and its bromide analogue as a function of temperature has been studied using neutron powder diffraction. Structural analysis reveals significant displacements of the basal oxygen of the central FeO_6 octahedra within the Fe–O triple perovskite block. The disorder is interpreted as rotations of the octahedra about the *c*-axis, necessary to reduce bond strain arising from the mis-match between the planar Fe–O bonds of octahedral and square pyramidal geometries. The degree of rotation is seen to increase on cooling indicating additional strain at low temperatures. The unit cell of $Pb_4Fe_3O_8Br$ shows the expected expansion, although results suggest the expanded Pb_2Br layer places increased compressive stress on the triple perovskite block which shows an appreciable contraction along the *c*-direction. Both materials exhibit a smooth thermal expansion with surprisingly little difference in the expansion rate of the tetragonal plane and the *c*-axis. Fitting the temperature dependence of the magnetic

intensity has allowed the $T_{Néel}$s to be determined as 610(5) K and 600(5) K for $Pb_4Fe_3O_8Cl$ and $Pb_4Fe_3O_8Br$ respectively. The magnetic cell is related to the nuclear structure by the transformation matrix (10/110/002) in an analogous fashion to Fe based YBCO derivatives. The ordered component of the Fe moments is high, $\sim 3.5\ \mu_B$ at room temperature, consistent with the presence of high spin Fe^{3+} a conclusion supported by the absence of oxygen deficiency within either material.

Acknowledgements

We thank the EPSRC for grant GR/M21836 in aid of this work and the ILL for provision of neutron facilities and technical help. The assistance of Dr A. J. Wright with the magnetic refinements was also appreciated.

References

1 R. C. Rouse, *Am. Mineral.*, 1971, **56**, 625.
2 J. Pannetier and P. Batail, *J. Solid State Chem.*, 1981, **39**, 15.
3 J. Emery, A. Cereze and F. Varret, *J. Phys. Chem. Solids*, 1980, **41**, 1035.
4 Q. Huang, P. Karen, V. L. Karen, A. Kjekshus, J. W. Lynn, A. D. Mighell, N. Rosov and A. Santoro, *Phys. Rev. B*, 1992, **45**, 9611.
5 J. Lindén, A. Kjekshus, P. Karen, J. Miettinen and M. Karppinen, *J. Solid State Chem.*, 1998, **139**, 168.
6 P. Karen, A. Kjekshus, Q. Huang, J. W. Lynn, N. Rosov, I. N. Sora, V. L. Karen, A. D. Mighell and A. J. Santoro, *J. Solid State Chem.*, 1998, **136**, 21.
7 R. J. Cava, P. Bordet, J. J. Capponi, C. Chaillout, J. Chenavas, T. Fournier, E. A. Hewat, J. L. Hodeau, J. P. Levy, M. Marezio, B. Batlogg and L. W. Rupp Jr., *Physica C*, 1990, **167**, 67.
8 L. Rukang, *J. Solid State Chem.*, 1997, **130**, 154.
9 L. Rukang, *Physica C*, 1997, **277**, 252.
10 M. J. Rey, P. Dehaudt, P. Joubert and A. W. Hewat, *Physica C*, 1990, **167**, 162.
11 O. Chmaissem, J. D. Jorgensen, H. Shaked, P. Dollar and J. L. Tallon, *Phys. Rev. B*, 2000, **61**, 6401.
12 R. J. Crooks, C. S. Knee and M. T. Weller, *Chem. Mater.*, 1998, **10**, 4169.
13 H. M. Rietveld, *J. Appl. Crystallogr.*, 1969, **2**, 65.
14 A. C. Larson and R. B. Von Dreele, MS-H805, Los Alamos National Laborotory, Los Alamos, NM 87545, 1994.
15 L. Koester, H. Rauch and E. Seymann, *At. Nucl. Data Tables*, 1991, **49**, 65.
16 P. J. Brown, in *International Tables for Crystallography*, ed. T. Hahn, Kluwer Academic Publishers, Dordrecht, 1992, vol. C.
17 D. Altermatt and I. D. Brown, *Acta Crystallogr., Sect. B*, 1985, **41**, 240.
18 M. T. Anderson, K. R. Poeppelmeier, J-P. Zhang, H-J Fan and L. D. Marks, *Chem. Mater.*, 1992, **4**, 1305.
19 A. C. McLaughin, W. Zhou, J. P. Attfield, A. N. Fitch and J. L. Tallon, *Phys. Rev. B*, 1999, **60**, 7512.
20 D. L. Corker, A. M. Glazer, J. Dec, K. Roleder and R. W. Whatmore, *Acta Crystallogr., Sect. B*, 1997, **53**, 135.
21 T. Yuen, M. Seyedahmadian, R. E. Salomon, G. H. Myer and G. Cao, *J. Appl. Phys.*, 1996, **79**, 6001.
22 R. D. Shannon, *Acta Crystallogr., Sect. A*, 1976, **32**, 751.